A&A, 697, A132 (2025)
https://doi.org/10.1051/0004-6361/202451470

Astronomy & Astrophysics

JWST/MIRI detects the dusty SN1993J about 30 years after explosion

Tamás Szalai[1,2,⋆], Szanna Zsíros[1], Jacob Jencson[3], Ori D. Fox[4], Melissa Shahbandeh[3,4], Arkaprabha Sarangi[5], Tea Temim[6], Ilse De Looze[7], Nathan Smith[8], Alexei V. Filippenko[9], Schuyler D. Van Dyk[10], Jennifer Andrews[11], Chris Ashall[12], Geoffrey C. Clayton[13], Luc Dessart[14], Michael Dulude[4], Eli Dwek[15,16], Sebastian Gomez[4], Joel Johansson[17], Dan Milisavljevic[18,19], Justin Pierel[4], Armin Rest[3,4], Samaporn Tinyanont[20,21], Thomas G. Brink[9], Kishalay De[22], Michael Engesser[4], Ryan J. Foley[20], Suvi Gezari[4], Mansi Kasliwal[23], Ryan Lau[24], Anthony Marston[25], Richard O'Steen[4], Matthew Siebert[4], Michael Skrutskie[26], Lou Strolger[4], Qinan Wang[3], Brian J. Williams[27], Robert Williams[4], Lin Xiao[28,29], and WeiKang Zheng[9]

(Affiliations can be found after the references)

Received 11 July 2024 / Accepted 12 March 2025

ABSTRACT

Context. Core-collapse supernovae (CCSNe) have long been considered to contribute significantly to the cosmic dust budget. Newly-formed dust in the SN ejecta cools quickly and is therefore detectable at mid-infrared (mid-IR) wavelengths. However, before the era of the *James Webb* Space Telescope (JWST), direct observational evidence for dust condensation was found in only a handful of nearby CCSNe, and dust masses ($\sim 10^{-2}$–10^{-3} $M_\odot$, generally limited to <5 yr and to >500 K temperatures) have been two to three orders of magnitude smaller than theoretical predictions and dust amounts found by far-IR/submillimeter observations of Galactic SN remnants and in the very nearby SN 1987A.

Aims. As recently demonstrated, the combined angular resolution and mid-IR sensitivity of JWST finally allow hidden cool (~100–200 K) dust reservoirs in extragalactic SNe beyond SN 1987A to be revealed. Our team received JWST/MIRI time for studying a larger sample of CCSNe to fill the currently existing gap in their dust formation histories. The first observed target of this program was the well-known Type IIb SN 1993J that appeared in M81.

Methods. We generated its spectral energy distribution (SED) from the current JWST/MIRI F770W, F1000W, F1500W, and F2100W fluxes. We fit single- and two-component silicate and carbonaceous dust models to the SED in order to determine the dust parameters.

Results. We find that SN 1993J still contains a significant amount (~0.01 $M_\odot$) of dust ~30 yr after explosion. Comparing our results to those from the analysis of earlier *Spitzer* Space Telescope data, we observed a similar amount of dust as was detected ~15–20 yr ago, but at a lower temperature (noting that the modeling results of the earlier *Spitzer* SEDs have strong limitations). We also found residual background emission near the SN site (after point-spread-function subtraction on the JWST/MIRI images) that may plausibly be attributed to an IR echo from more distant interstellar dust grains heated by the SN shock-breakout luminosity or ongoing star formation in the local environment.

Key words. supernovae: general – dust, extinction – ISM: supernova remnants – supernovae: individual: SN1993J

1. Introduction

Core-collapse supernovae (CCSNe), the energetic final explosions of evolved massive ($\gtrsim 8\,M_\odot$) stars, offer unique possibilities to (i) study extreme physical processes, (ii) uncover details about pre-explosion stellar evolution, and (iii) measure cosmic distances. While most CCSNe fade over the course of several months to years, the *Spitzer* Space Telescope (*Spitzer*) "Warm" (post-cryogenic) mission (i.e., 3.6 and 4.5 μm) highlighted a subset of dusty SNe that can remain bright for many years, even decades, post-explosion (e.g., Fox et al. 2010, 2011, 2013; Tinyanont et al. 2016; Szalai et al. 2019, 2021). The increased sensitivity of the *James Webb* Space Telescope (JWST) and its access to even longer wavelengths (e.g., 25 μm) has resurrected the SN community's interest in such dusty objects. The origin and heating mechanism of the dust can have several important implications. If the dust is newly formed in the ejecta, the inferred dust masses could provide the much sought-after evidence supporting SNe as significant sources of dust in the Universe (e.g., Dwek et al. 2007). If there is also or only pre-existing dust in the circumstellar medium (CSM) at the time of explosion, it can be used as a proxy to trace the pre-SN mass-loss history and constrain the progenitor system (e.g., Fox et al. 2011).

Up to the beginning of the JWST era, there had only been a few objects also observed at longer mid-IR wavelengths: several Type II-P SNe up to a few years old (e.g., Kotak et al. 2009; Fabbri et al. 2011; Meikle et al. 2011; Szalai et al. 2011; Szalai & Vinkó 2013) and older objects such as SNe 1978K (Tanaka et al. 2012), 1980K (Sugerman et al. 2012) and 1995N Van Dyk (2013). However, only the famous nearby SN 1987A in the Large Magellanic Cloud was able to be studied in detail by *Spitzer* (Bouchet et al. 2006; Dwek et al. 2010; Arendt et al. 2020) as well as in the far-IR/submillimeter regime (via *Herschel* and ALMA, see Matsuura et al. 2011, 2019; Indebetouw et al. 2014). Thus, for the most dusty extragalactic SNe, we have no information on temperatures $\lesssim$150 K, where the bulk of the dust is thought to reside – as was also shown by recent far-IR and submillimeter observations of old Galactic SN remnants (SNRs), such as Cassiopeia A (Barlow et al. 2010; Sibthorpe et al. 2010; Arendt et al. 2014) and the Crab (Gomez et al. 2012; Temim & Dwek 2013; De Looze et al. 2019). A number of questions remain, and the phase space of such observations (in terms of mass/temperature of dust versus SN age) remains relatively

⋆ Corresponding author: szaszi@titan.physx.u-szeged.hu

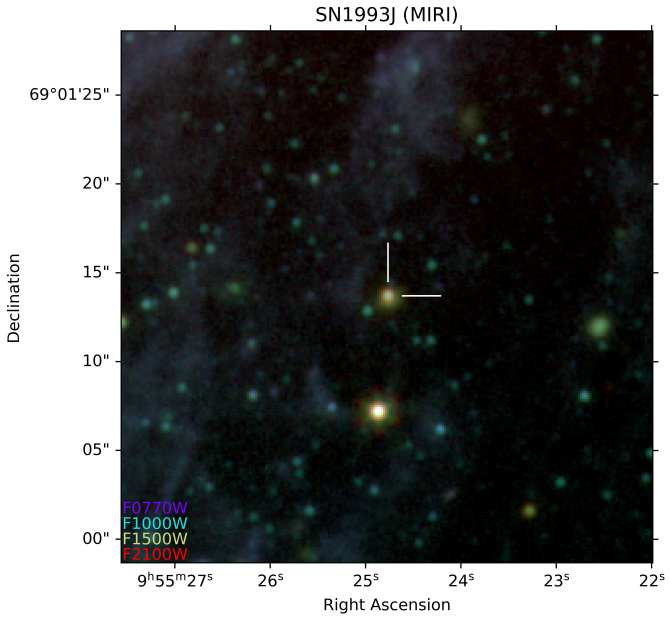

Fig. 1. JWST/MIRI composite image of SN 1993J [$\alpha(2000) = 09^h55^m24.778^s$, $\delta(2000) = +69°01'13''.70$] obtained on 2024 February 13.6 UTC (11 280 days post-explosion). The white tick marks show the position of the target.

unpopulated. Moreover, it should be noted that while *Spitzer* had good mid-IR sensitivity, its angular resolution was too poor to separate most extragalactic SNe from their nearby host-galaxy emission in star-forming regions and H II regions, among others (especially at $\lambda \gtrsim 20\,\mu$m).

Importantly, JWST offers a new opportunity to detect the late phases of cool (~100–200 K) dust in extragalactic SNe beyond SN 1987A. JWST has the potential to detect (i) cooler dust grains at wavelengths greater than 4.5 μm, (ii) the 10 μm silicate feature that can distinguish grain compositions, and (iii) faint emission from SN at very late epochs that would have gone undetected by *Spitzer* and any other mid-IR spacecraft. Only a few months after the start of its scientific mission, JWST achieved important results in this field. Our team has already detected a significant amount of cool dust in SNe IIP 2004et and 2017eaw (Shahbandeh et al. 2023) as well as in SN IIL 1980K (Zsíros et al. 2024). In SN 2004et, the observations have uncovered the largest newly formed ejecta dust masses in an extragalactic SN other than SN 1987A, with $\gtrsim 10^{-2}\,M_\odot$ of dust at a temperature of ~140 K.

In this paper, we present JWST observations of another nearby famous event, SN 1993J. This object is the prototype of Type IIb explosions, which form a transitional group between H-rich Type II and H-free Type Ib/c CCSNe (see, e.g., Filippenko 1988, 1997; Filippenko et al. 1993; Nomoto et al. 1993) and constitute about 10% of CCSNe (Smith et al. 2011). Due to its proximity (3.63 ± 0.31 Mpc; Freedman et al. 2001) and its fortunate location in the outskirts of its host galaxy M81, SN 1993J has become one of the best-observed SNe, possessing various long-term multiwavelength datasets and detailed analyses published in the literature. We also know much about its progenitor system. The exploding star, likely a K0-type red supergiant (RSG), was directly identified in pre-explosion images (Aldering et al. 1994; Cohen et al. 1995) and had disappeared years after explosion (Maund & Smartt 2009). The progenitor may have been a member of a massive binary system (Maund et al. 2004) with a hotter (B2 type) companion that was likely directly detected (Fox et al. 2014).

In addition, SN 1993J has shown various signs of ongoing interaction between the shock and the CSM from early to late phases in the optical, radio, and X-ray bands (e.g., Matheson et al. 2000; Weiler et al. 2007; Chandra et al. 2009; Smith et al. 2017); see Zsíros et al. (2022, hereafter Z22) for a recent review). We note that SN 1993J is one of the very few extragalactic SNe besides SN 1987A where, via very-long-baseline radio interferometry, it was possible to resolve how the expanding SN shock is running into the CSM (Bietenholz et al. 2001, 2003; Bartel et al. 2002). Signs of dust formation have been published based on early-time near-IR observations (Matthews et al. 2002) and late-time optical spectral analysis (Smith et al. 2017; Bevan et al. 2017). In Z22, some of us presented a detailed analysis of the complete *Spitzer* mid-IR light curve (LC) and spectral energy distribution (SED) and modeling of the object (part of the *Spitzer* LC was also published by Tinyanont et al. 2016).

With the recent JWST data, SN 1993J has become one of the few SNe for which a dust-formation history can be followed during the first decades after explosion. In Sect. 2, we describe the steps of data reduction, while Sect. 3 presents the results of our analysis based on modeling the recent mid-IR SED. We discuss our findings in Sect. 4 and summarize our conclusions in Sect. 5.

2. Observations and data reduction

The JWST observing program #3921 (PI O. D. Fox)[1] is designed as a survey to image a large, diverse sample of SNe with the Mid-Infrared Instrument (MIRI; Bouchet et al. 2015; Ressler et al. 2015; Rieke et al. 2015; Rieke & Wright 2022). The observations are being acquired in the F770W, F1000W, F1500W, and F2100W filter bands using the FASTR1 readout pattern in the full array mode and a four-point extended source dither pattern. A description of our detailed calibration process of the JWST/MIRI images was recently published by Shahbandeh et al. (2023). To align JWST and *Hubble* Space Telescope (HST) images of the fields (when available) with each other, we used the JWST HST Alignment Tool (JHAT; Rest et al. 2023).

The first observed target of the SURVEY 3921 program was SN 1993J. The MIRI images were obtained on 2024 February 13.6 UTC (11 280 days after explosion, t_0 = 49074.0 MJD, Lewis et al. 1994). The SN can be identified as a clear and bright point source at all wavelengths from 7.7 to 21.0 μm (see a composite image of the field in Fig. 1).

To measure the fluxes of SN 1993J in JWST/MIRI images, we followed the method described in detail by Shahbandeh et al. (2023). We performed point-spread-function (PSF) photometry on background-subtracted level-two data products using `WebbPSF` (Perrin et al. 2014) implemented in the `space-phot` package[2] (Pierel 2024). We experimented with multiple PSF sizes in the fitting, and they variably resulted in underestimation or overestimation of the local background emission. The resulting fluxes of all four dithers of each filter were then averaged, and we incorporated the variations seen from using multiple PSF sizes into our estimates of the measurement uncertainties. We examine the local background emission from the PSF-fitting residuals in more detail in Sect. 3.3. The total

[1] https://www.stsci.edu/jwst/science-execution/program-information?id=3921
[2] https://zenodo.org/records/12100100

Table 1. JWST/MIRI AB magnitudes and fluxes of SN 1993J on 2024 February 13.6 UTC (day 11 280 post-explosion).

Filter	AB mag	F_ν (μJy)	F_λ erg s^{-1} cm^{-2} Å^{-1}
F770W	20.52 ± 0.04	22.5 ± 1.0	$(1.14 \pm 0.04) \times 10^{-19}$
F1000W	19.88 ± 0.05	40.6 ± 1.9	$(1.22 \pm 0.06) \times 10^{-19}$
F1500W	18.39 ± 0.18	160.0 ± 26.5	$(2.13 \pm 0.35) \times 10^{-19}$
F2100W	17.43 ± 0.06	387.3 ± 21.4	$(2.63 \pm 0.15) \times 10^{-19}$

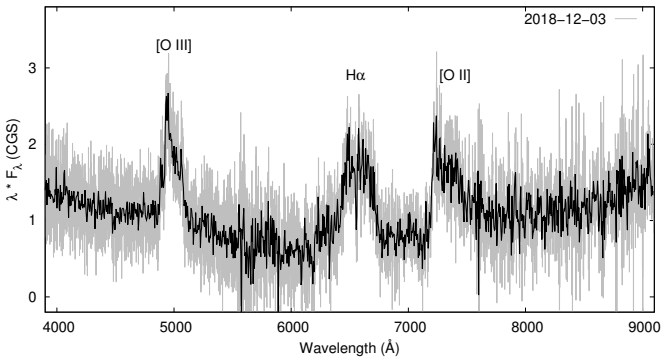

Fig. 2. High-resolution optical spectrum of SN 1993J obtained with Keck/LRIS on 2018 December 3, 9381 days after explosion. The dark solid line marks the five Å-binned data.

(Galactic + host) reddening value of $E(B-V) = 0.19 \pm 0.09$ mag (Richardson et al. 2006) implies that the extinction is negligible in the mid-IR range. The final results of our JWST/MIRI photometry of SN 1993J are presented in Table 1.

During the analysis described in Sect. 3.2, we also used a single unpublished late-time optical spectrum of SN 1993J obtained with the Keck Low Resolution Imaging Spectrometer (LRIS; Oke et al. 1995) on 2018 December 3 (at epoch 9381 days; see Fig. 2). The spectrum was acquired with the slit oriented at or near the parallactic angle to minimise slit losses caused by atmospheric dispersion (Filippenko 1982). The LRIS observation utilized the 1″-wide slit, 600/4000 grism, and 400/8500 grating to produce a similar spectral resolving power ($R \approx 700$–1200) in the red and blue channels. Data reduction followed the standard techniques for CCD image processing and spectrum extraction using the LPipe data-reduction pipeline (Perley 2019). Low-order polynomial fits to comparison-lamp spectra were used to calibrate the wavelength scale, and small adjustments derived from night-sky lines in the target frames were applied. The spectrum was flux calibrated using observations of appropriate spectrophotometric standard stars observed on the same night at similar airmasses and with an identical instrument configuration.

3. Analysis

3.1. Modeling of the mid-IR SEDs of SN 1993J

The mid-IR (continuum) excess relative to the Rayleigh-Jeans tail in the late-time SED of an SN typically indicates the presence of dust. As described above, this dust may be (i) newly formed, in either the inner unshocked ejecta or in the cool dense shell (CDS) of post-shocked gas lying between the forward and reverse shocks, and/or (ii) pre-existing, that is, formed in a steady wind from the progenitor or during a short-duration pre-SN outburst. In either case, different heating mechanisms, geometries, grain composition and size distributions, and dust clumpiness effects should be taken into account to find a proper description of the physical background of the observed mid-IR radiation (see more details provided by, e.g., Shahbandeh et al. 2023, and references therein).

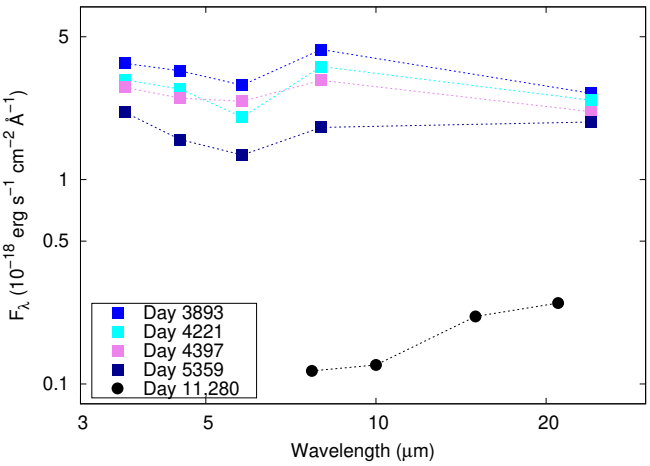

Fig. 3. Evolution of observed mid-IR SEDs of SN 1993J between 2003 and 2024. Color squares and black circles denote *Spitzer*/IRAC+MIPS (Zsíros et al. 2022) and JWST/MIRI data points, respectively.

A detailed analysis of the properties of the dust content and its possible origin and heating effects is described by Z22, based on the full *Spitzer* dataset of the event obtained between 2003 and 2019 (10–26 yr after explosion). The study concluded that all the dust suggested by *Spitzer* data can be newly formed and is located in the inner ejecta and/or in the CDS. This picture is also strengthened by the modeling of red-blue line-profile asymmetries found in late-time optical spectra of the object (Bevan et al. 2017; Smith et al. 2017). At the same time, the results of Z22 also allow for the presence of pre-existing dust, heated collisionally by hot gas in the reverse shock (assuming a possible range of 5000–15 000 km s^{-1} for the shock velocity) or (more likely) radiatively by energetic photons from shock-CSM interaction.

We did not repeat all the steps presented by Z22 here. However, we examined (i) the validity of the conclusions of the previous work and (ii) the points where new JWST data allowed us to carry out an even more detailed analysis.

First, we compared the fluxes of SN 1993J measured by JWST/MIRI (day 11 280 post-explosion) to those measured by *Spitzer* (between days 3893 and 5359) and published by Z22. The evolution of the mid-IR SEDs of the object between days 3893 and 11 280 is shown in Fig. 3. The JWST fluxes are an order of magnitude lower than the earlier ones, and the shape of the SED seems to shift toward lower temperatures. We note that there are further *Spitzer*/IRAC 3.6 and 4.5 μm data up to ∼9650 days. The SN shows continuously decreasing fluxes at both wavelengths (see Tinyanont et al. 2016; Z22). We also note that recent JWST imaging strengthens our previous assumption that the environment of SN 1993J is relatively smooth and has a low local IR background (see Fig. 1), and it gives further justification for the reliability of our previously published *Spitzer* photometry (there was no possibility for subtracting pre-explosion images; see Z22).

Next, we carried out simple analytic modeling of the JWST/MIRI SED of SN 1993J described by Hildebrand (1983) (similarly to the work of Z22 on *Spitzer* SEDs). This method assumes only the thermal emission of an optically thin dusty

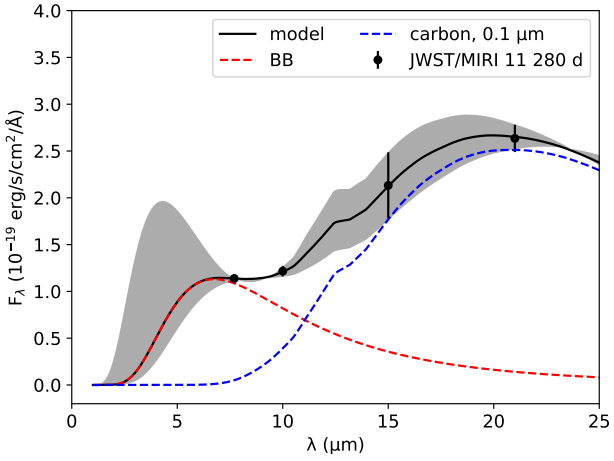

Fig. 4. Best-fit two-component – cold ($T_{\rm cold} \approx 120$ K) amC dust plus hot ($T_{\rm hot} \approx 430$ K) BB – model fit to the four-point JWST/MIRI SED of SN 1993J (day 11 280). Gray regions pertain to models fit to the upper and lower constraints on the fluxes based on the photometric uncertainties, respectively. Model parameters are shown in Table 2. Filled circles denote measured fluxes. The hot component was replaced also by a fixed $T = 1000$ K BB and a power-law function, causing no significant changes in the parameters of the cold dust component (see details in the text).

shell at a single equilibrium temperature T_d, with a dust mass of M_d and particle radius of a. The observed flux of the dust can be written as

$$F_\lambda = M_d B_\lambda(T_d)\kappa(a)/D^2, \quad (1)$$

where $B_\lambda(T_d)$ is the Planck function, $\kappa(a)$ is the dust mass absorption coefficient, and D is the distance to the source.

For building the model SEDs, we calculated filter-integrated fluxes using Eq. (1) convolved with the JWST/MIRI filter transmission profiles and fit them to the JWST data. We note that while our group (Shahbandeh et al. 2023) adopted a more general formalism from Dwek et al. (2019) allowing for the presence of optically thick dust, here we focused only on the optically thin case because of the decades-long age of the SNR (just as we did in the case of SN 1980K; Zsíros et al. 2024). We also note that using only Eq. (1) did not allow us to take into account various geometries or clumpiness factors. This avoided the overinterpretation of a four-point SED and led us to draw conclusions based on the parameters determined from the simplest assumptions. Nevertheless, we had to handle all the constraints of this model carefully.

From the previously published *Spitzer* dataset, it was difficult to infer the dust composition in SN 1993J. These data do not cover the 8–24 μm range (except for a single noisy *Spitzer*/IRS spectrum obtained in 2008), which could have been critical for disentangling the spectral features of Si-rich and carbonaceous dust. Thus, in Z22, both amorphous carbon (amC) and silicate dust models were fit to the *Spitzer* SEDs. In the case of the current JWST dataset, fluxes measured with the F1000W, F1500W, and F2100W filters could be more helpful in revealing the true dust composition.

Following Shahbandeh et al. (2023), the absorption and emission properties for amC and silicate grains were obtained from Zubko et al. (2004) and Draine & Li (2007), respectively (see Sarangi 2022 for the values of absorption coefficients κ_λ). As a first step, we applied a 0.1 μm grain size, just as we did before in our previous JWST/MIRI data papers (Shahbandeh et al. 2023; Zsíros et al. 2024) (as also done by Z22 for the *Spitzer* data analysis of SN 1993J). We found that the four-point day 11 280 JWST/MIRI SED of SN 1993J cannot be properly fit with any single-component amC or silicate dust models. While the measured 7.7 μm flux appears to show an excess with respect to each single-component model, we added a hot blackbody (BB) component and obtained an adequate fit assuming a cold amC dust component associated with a hot BB (see Fig. 4). The $a = 0.1$ μm silicate models did not result in reasonable fits, even in the two-component cases.

Following our referee's advice, we also performed the SED fitting assuming larger ($a = 1.0$ and 5.0 μm) grain radii. We found that even this choice does not allow us to find good single-component solutions. Nevertheless, two-component models worked if we used $a = 1.0/5.0$ μm amC or $a = 5.0$ μm silicate dust associated with a hot BB (see Fig. A.1). We note, however, that such large grains are not expected in SNe at this phase (especially in SNe IIb; see Sect. 4). Furthermore, this dataset did not allow us to truly disentangle models with different grain-size distributions. Thus, from now on, we refer to the results of the original fit assuming a cold $a = 0.1$ μm amC dust plus a hot BB.

Since fitting a two-component model to only four SED points leads to unphysically low parameter uncertainties, we repeated the fit based on the upper and lower constraints placed on the JWST/MIRI fluxes by the photometric uncertainties in Table 1. Thus, the cold dust component has an inferred mass of $M_{\rm cold} = (8.9^{+4.5}_{-2.3}) \times 10^{-3}$ M$_\odot$ and a temperature of $T_{\rm cold} = 116 \pm 10$ K. For the average flux values, we also calculated the luminosity and the BB radius of the cold components (i.e., the minimum size of an optically thin, spherical dust-forming region), finding $L_{\rm cold} \approx 1.0 \times 10^{38}$ erg s^{-1} and $R_{\rm BB,cold} \approx 1.3 \times 10^{16}$ cm. As Fig. 3 already suggested, the current value of $L_{\rm cold}$ is well below what has been measured from *Spitzer* SEDs from $\gtrsim$5 yr prior ($(10.0–15.6) \times 10^{38}$ erg s^{-1}; see Z22).

As can be recognized from Fig. 4, how the assumed hot component affects the parameters of the cold dust component can be an important question here. A similar hot gas/dust component has previously been detected in other decades-old SNe such as SN 1980K (Zsíros et al. 2024), SN 1987A (Dwek et al. 2010; Arendt et al. 2016, 2020), and SN 2004et (Shahbandeh et al. 2023). The general assumption is ongoing circumstellar interaction in the close environment of these SNe, and this is the case for SN 1993J as well. As mentioned above, SN 1993J has shown various signs of CSM interaction, and based on long-term monitoring of its optical spectra, this level remains strong even ~20 yr after explosion (see Milisavljevic et al. 2012; Smith et al. 2017, and Fig. 5 of this work).

Nevertheless, based on JWST data alone, we cannot conclusively determine the current temperature of the hot component. Unfortunately, we are not aware of any near-IR data from the past few years (the last *Spitzer* data at 3.6 and 4.5 μm were obtained in 2019; however, the SN was then very faint at these wavelengths, so we are unable to follow the real steepness of its decline after that point). If we fit our two-component model using free parameters, we get $T_{\rm hot} = 430^{+150}_{-50}$ K for the temperature of the hot component. Between days 3893 and 5359, we did not observe a clear evolution of $T_{\rm hot}$ (its value varies between 640 and 780 K; see Z22). However, we note that these SEDs are also unconstrained below 3.6 μm. Thus, following the method described by Zsíros et al. (2024), we repeated the fitting procedure, fixing $T_{\rm hot} = 1000$ K to see how it affects the parameters of the cold dust component. As shown in Table 2, these differences are essentially small. Since the nature of the hot component is not necessarily thermal, we also ran a test assuming that the hot

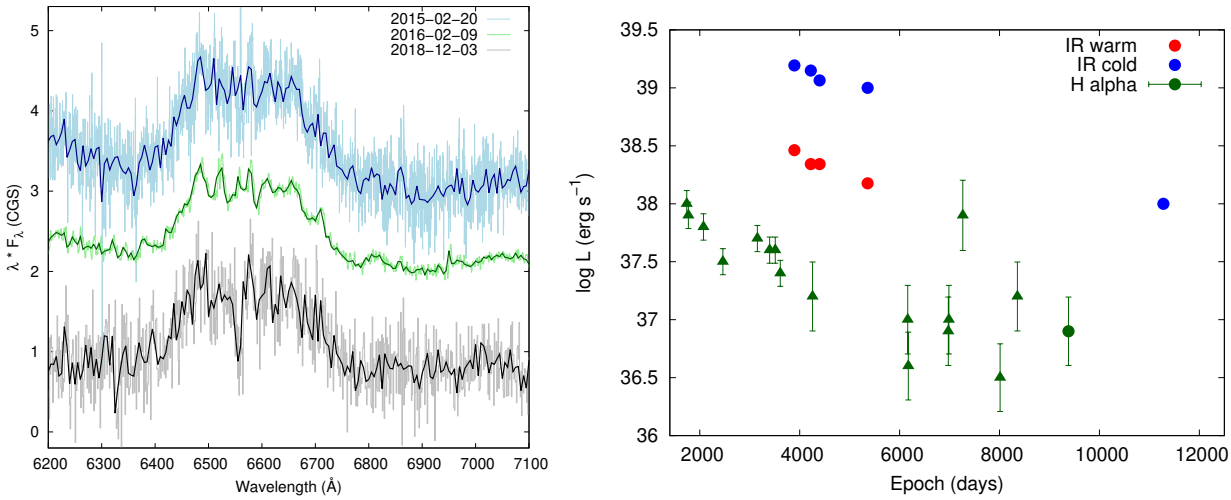

Fig. 5. Comparison of late-time Hα and IR emission of SN 1993J. *Left:* Hα emission line profiles in the most recent high-resolution optical spectra of SN 1993J obtained with Keck/LRIS in 2015, 2016 (published by Smith et al. 2017), and in 2018 (this work). The dates belong to epochs 7999, 8353, and 9381 days, respectively. Spectra are vertically shifted for better comparison. Dark solid lines mark the five Å-binned datasets. *Right:* Long-term luminosity evolution of warm and cold dust components (Z22 and this work) compared to Hα line luminosities (circle: this work; triangles: adopted from Smith et al. 2017) produced dominantly by the part of the SN ejecta crossing and being excited by the reverse shock.

Table 2. Parameters of the best-fit two-component (cold amC dust + hot BB) models for the day 5359 *Spitzer* and the day 11 280 JWST/MIRI SED of SN 1993J. Both models were calculated using κ files from Sarangi (2022).

Data	Epoch (days)	$T_{\rm cold}$ (K)	$M_{\rm cold}$ (10^{-3} M$_\odot$)	$L_{\rm cold}$ (10^{38} erg s^{-1})	$R_{\rm BB,cold}$ (10^{16} cm)	$T_{\rm BB,warm}$ (K)
Spitzer (3.6–8.0 + 24 μm)	5359	167 ± 4	14.3 ± 2.9	10.0	2.9	901 ± 52
JWST (7.7, 10.0, 15.0, 21.0 μm)	11 280	116 ± 10	$8.9^{+4.5}_{-2.3}$	1.0	1.3	430^{+150}_{-50}
		128 ± 2	5.2 ± 0.5	–	–	1000 (fixed)

component has a power-law nature ($F_\lambda \propto \lambda^{0.3}$, fit to the day 5359 3.6–5.8 μm *Spitzer* fluxes). However, in this case, we observed that this function declines quickly below $\sim 10^{20}$ erg s^{-1}cm^{-2} Å^{-1} beyond 10 μm. Thus, its influence on the cold dust component is even smaller than that of the tested hot dust/BB components.

We note that Z22 used older absorption coefficients during the modeling of *Spitzer* SEDs. Hence, for an improved comparison, we also repeated the fitting of two-component amC dust models to the last (day 5359) *Spitzer* SED using the κ values adopted from Sarangi (2022). Results of this repeated fitting are shown in Table 2. We discuss in detail the evolution of dust parameters in Sect. 4.

Furthermore, we examined the potential contribution of the long-wavelength synchrotron radiation to the mid-IR SED (emerging from shock-CSM interaction), just as was done recently by Larsson et al. (2023) and Jones et al. (2023) in the case of SN 1987A. Since SN 1993J has also been a target of long-term radio observations, we followed their method and extrapolated the radio LC model parameters of SN 1993J from Weiler et al. (2007) (see their Eq. (1), including both nonthermal synchrotron self-absorption and thermal free-free absorbing components) to the mid-IR range at the epoch of 11 280 days. We found that the original model values may give a $\lesssim$10 μJy contribution at 25.5 μm and even lower amounts at shorter wavelengths. We also note that the real contribution may be even smaller since the general model of Weiler et al. (2007), as the authors discussed, gives an overestimation of the measured radio fluxes after ~3000 days (the achromatic break in the radio LCs of SN 1993J was also described by, e.g., Martí-Vidal et al. 2011; Kundu et al. 2019). So unlike in the case of SN 1987A, the contribution of the synchrotron emission to the very late time mid-IR SED of SN 1993J seems to be negligible.

3.2. Comparison of late-time multiwavelength data

It is also worth comparing the mid-IR evolution of SN 1993J to published late-time UV/optical flux changes (see e.g. Fransson & Kozma 2002; Dessart & Hillier 2022; Dessart et al. 2023). This step could help reveal the role of CSM interaction in the potential heating of the dust content of the SN shown by recent JWST measurements. We therefore examined the late-time HST photometry of the object. Based on the results presented by Baer-Way et al. (2024) – which also contain previously published data from Van Dyk et al. (2002) and Fox et al. (2014) – the F336W fluxes show a moderate decline by 0.026 and 0.036 mag (100 d)$^{-1}$ in the ranges 6903–8022 d and 8022–10 123 d, respectively. In the F814W filter, there is a steeper decline of 0.073 mag (100 d)$^{-1}$ during days 6903–10 123, which is preceded by a slower decrease of 0.029 mag (100 d)$^{-1}$ during days 2990–6903. However, we note that these decline rates are determined from single pairs of data points.

We also performed a similar analysis of previously published well-sampled *Spitzer*/IRAC LCs (Tinyanont et al. 2016; Z22). While there are 3.6 and 4.5 μm data up to ~9600 days, the object seems to fade into the background at these wavelengths after ~5500 days. Thus, we only used data of days 3875–5345, and we determined a decline of 0.039, 0.057, 0.060, and

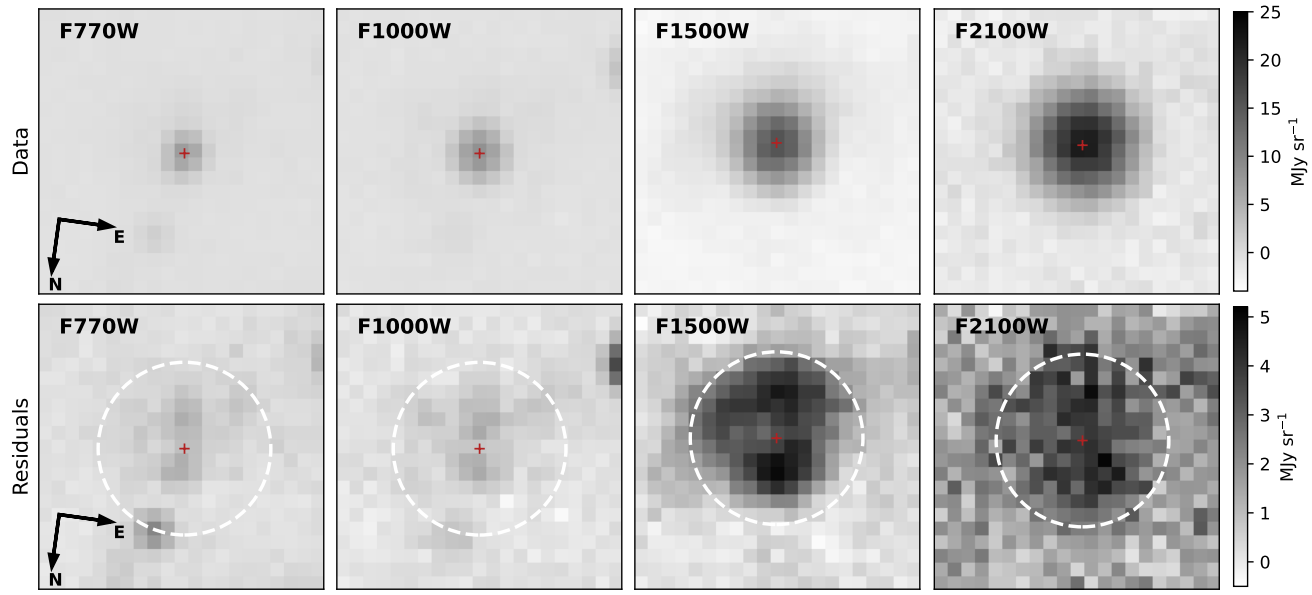

Fig. 6. Background emission in the JWST/MIRI images of SN 1993J after removing the bright SN component. *Top:* Location of SN 1993J in each of the four filters of MIRI imaging. The red cross indicates the centroid of the SN in each panel obtained from our PSF-fitting photometry. We note that the photometry was performed on individual dithered exposures, but here the pixels around the SN position have been median combined for display purposes. *Bottom:* Background emission around the position of SN 1993J in the four MIRI filters after the removal of the bright SN source during PSF-fitting photometry. In each case, the background level immediately under the SN was determined by fitting a small box (width of five pixels). The fits were repeated with a larger box while holding the background fixed to subtract the SN PSF. As in the top row, the residual data from each dither have been median combined for display purposes, and the red cross indicates the centroid of the SN PSF. The white dashed circle is 0.″7 in radius from this position.

0.071 mag $(100\,\mathrm{d})^{-1}$ for 3.6, 4.5, 5.8, and 8.0 μm *Spitzer* LCs, respectively. While *Spitzer* data have quite large uncertainties (0.2–0.3 mag), it seems that fading is slower at shorter wavelengths. The decline rate of HST F814W data during days 2990–6903 also fits this trend (see Baer-Way et al. 2024). This seems to further strengthen the importance of the ongoing CSM interaction in the environment of SN 1993J.

Using the data published by Z22 and the decline rates reported above, we also undertook an extrapolation of the 8.0 μm *Spitzer*/IRAC LC to day 11 280 (17.25 mag) and compared this extrapolated 8.0 μm value to the measured JWST/MIRI 7.7 μm brightness (16.19 mag, with both values in Vega magnitudes). While the difference between the spatial resolution of the two telescopes and the (slightly) different transmission curves of the two filters make us cautious, we suggest that the ∼1 mag difference really implies a slowing decline rate after day 5345.

Finally, we refer to the results of Smith et al. (2017), who give the long-term evolution of Hα luminosities of SN 1993J (they also adopted earlier-time data from Chandra et al. 2009). They found a slow continuous decline of log $L_{\mathrm{H}\alpha}$ from $\sim 10^{38}$ to $\sim 10^{37}$ erg s^{-1} during days ∼2000–8300 days. We note, however, that while line profiles seem to be similar, log $L_{\mathrm{H}\alpha}$ values show a large scatter after ∼6000 days. We highlight here that the breadth of the late-time Hα feature ($v \gtrsim 5000$ km s^{-1}) causes the gas in SN 1993J to be associated with ejecta excited by the reverse shock. This situation is different from the strongly interacting SNe IIn, where the persistent Hα emission ($v \lesssim 2500\,\mathrm{km\,s^{-1}}$) is associated the with progenitor wind swept up by the forward shock (see a detailed description by, e.g., Smith et al. 2017; Milisavljevic & Fesen 2017). We added one more point measured from the previously unpublished Keck/LRIS optical spectrum obtained at the epoch of day 9381 (see Sect. 2), which also seems to fit into this trend (we applied a 30% uncertainty for the calculated line flux, following the Smith et al. 2017 estimation of earlier Keck/LRIS data). Figure 5 shows the comparison of Hα line luminosities and IR luminosities calculated from cold and warm dust SED components (the latter values are adopted from Z22). The declining trends of all of these curves seem similar, which may suggest that longstanding (but continuously weakening) interaction has a role in heating both cold and warm dust components in the environment of SN 1993J. We discuss the details of possible dust-heating mechanisms in Sect. 4.

3.3. Local background emission at the SN site: Star formation or an IR echo

As described above in Sect. 2, we also examined the local background environment of SN 1993J based on our detailed photometric PSF-fitting analysis. The morphology and integrated fluxes of the residual emission are largely robust for appropriate choices of box sizes during the PSF-fitting procedure. Originally, we first fit the SN with the background flux as a free parameter using a small box (with a width of five pixels) so that the underlying background is approximately uniform. Then, we fixed the background level to this value and used a larger (21-pixel) box to allow us to integrate the total residual fluxes with the SN removed. In Fig. 6, we show the residual emission after removal of the PSF profiles obtained from these fits. The background emission is apparent in all four filters, with the strongest emission at F1500W and F2100W. Comparison with the higher resolution F770W and F1000W suggests the emission may be the result of a combination of multiple blended point-like sources as well as extended sources. To test the robustness of this procedure, we repeated it with small box sizes of five, seven, and nine pixels, and large box sizes of 15, 19, and 21 pixels, and we found generally consistent results for the integrated residual fluxes of

F1500W = 0.11 ± 0.01 mJy and F2100W = 0.14 ± 0.01 mJy. As shown in Appendix B (Fig. B.2), using too large of a box for the first fit such that the background residuals are nonuniform within the fitting region results in a spurious ring-like morphology due to oversubtraction of the core of the PSF.

Based on a simple BB fit to the residual fluxes and upper limits, the nature of the detected background emission seems to be consistent with dust at ~190 ± 20 K (see Appendix B for more details). The heating source of this dust could be local ongoing star formation in the vicinity of SN 1993J or, alternatively, a thermal IR echo powered by the SN itself.

We note that Sugerman & Crotts (2002) and Liu et al. (2003) identified optical light echoes (LEs) in HST images obtained in 2001. These LEs are assumed to scatter from interstellar dust sheets lying ~80 and ~220 pc in front of the SN, respectively. The bulk of the emission in the JWST/MIRI F1500W and F2100W images is within <0.7″, which is firmly below the radii of the two known optical echoes (~1.15″ and ~1.85–1.95″). Thus, this emission would correspond to a new echo from dust that, given a delay time of 31 yr, lies largely behind the SN at physical distances of ~5–13 pc (see, e.g., Eq. (1) of Dwek & Arendt 2008 for the relevant light-echo geometry). We note here that similar but more extended IR echoes have been observed around the Galactic SNR Cassiopeia A (Cas A; ~150 K, e.g., Krause et al. 2005; Dwek & Arendt 2008), which has been found to be the result of a SN 1993J-like Type IIb explosion that occurred ~350 yr ago (Krause et al. 2008). Dwek & Arendt (2008) found that a short (~1 day) burst of UV radiation with a luminosity of $\sim 1.5 \times 10^{11}$ $L_\odot$ from the SN shock breakout was needed to power the observed Cas A echo spectra from dust lying ~50 pc from the SN. Given the proximity of the dust in the case of SN 1993J, even a less extreme burst could plausibly power the observed emission as an IR echo, but a detailed examination of this possibility is beyond the scope of this work. Additional observations to better constrain the spectrum of the emission or detect variations in its apparent size or brightness would be necessary, for example, to characterize or rule out contributions from ongoing local star formation to heating of the dust.

4. Discussion

As presented above, the model fitting of the current JWST/MIRI SED is consistent with the presence of carbonaceous rather than Si-dominated dust, and this was not as clear from the earlier-phase (3893–5359 days) *Spitzer* data (Z22). Thus, assuming the presence of pure amC dust in SN 1993J and applying updated κ values (Sarangi 2022) for the recent JWST and earlier *Spitzer* data, we obtained a similar amount (~0.01 $M_\odot$) of dust for now as for ~15 yr ago (see Table 2). Figure 7 shows the determined dust masses in SN 1993J compared to other literature values based on mid-IR SED analyses.

We note, however, that the modeled SED parameters determined from the previously obtained *Spitzer* data should be handled carefully since the 8–24 μm range was not covered then and the spatial resolution of data at those wavelengths is also lower (especially that of the MIPS 24 μm images). Moreover, given the lack of any high-quality mid-IR spectra of SN 1993J (or any other SNe of similar type and age), the line-emission contribution to the measured fluxes is also still uncertain. Nevertheless, it seems that the temperature of the cold dust component is significantly lower now than it was ~15 yr ago (~120 K versus ~165 K; see Table 2) – but we again note that the modeling results of the *Spitzer* SEDs have strong limitations.

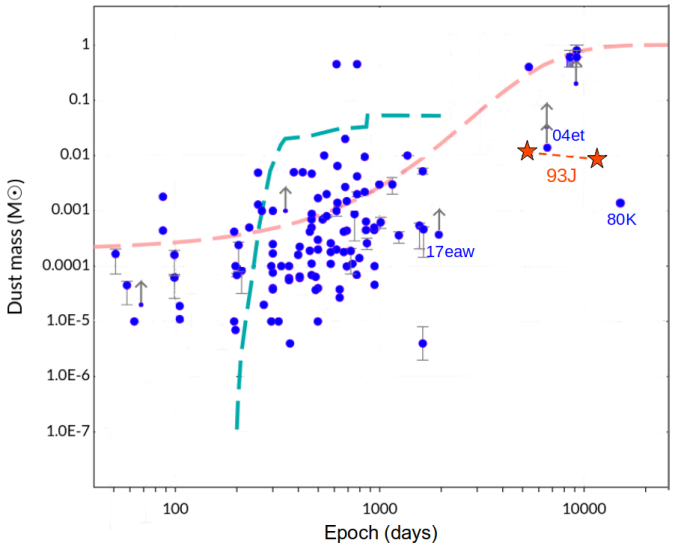

Fig. 7. Compilation of literature values for dust mass determinations based on mid-IR SED analyses in several individual CCSNe. The orange stars mark the dust masses of SN 1993J determined during this work. Other blue labels mark the cases of SNe IIP 2004et, 2017eaw (Shahbandeh et al. 2023), and SN IIL 1980K (Zsíros et al. 2024), where the estimated dust masses are also based on the recent analyses of JWST/MIRI SEDs. Dashed lines show examples of rapid (turquoise line, Sarangi & Cherchneff 2015) and steady continuous (pink line, Wesson et al. 2015) dust-formation theories. The source of the original interactive diagram is Roger Wesson's homepage (https://nebulousresearch.org/dustmasses/).

As shown in Table 2, we calculated the current luminosity of the cold dust component and obtained $L_{\rm cold} \approx 1.0 \times 10^{38}$ erg s^{-1}. This value, while definitely lower than ~15 yr ago, is still far above the total luminosity expected from the radioactive decay of ^{44}Ti + ^{57}Co + ^{60}Co (a total of 10^{36}–10^{37} erg s^{-1}), which is assumed to be the dominant energy source in CCSN ejecta for several years or decades after explosion (see, e.g., Tanaka et al. 2012; Seitenzahl et al. 2014). Thus, an extra energy source is needed to heat the ejecta dust up to the observed temperature. The known longstanding CSM interaction in the environment of SN 1993J is the primary explanation. As we show in Fig. 5, mid-IR luminosities have a long-term evolution very similar to what has been measured in Hα, and the latter is a well-known tracer of the level of shock-CSM interaction. Furthermore, we note that the majority of the interaction luminosity emerges in the form of X-ray and UV photons. As was shown by Smith et al. (2017), in the case of some strongly interacting SNe, the X-ray luminosity can achieve a factor of approximately ten higher level than the optical (Hα) luminosity. Thus, since the latest measured $L_{\rm H}\alpha$ values of SN 1993J are in the range $10^{36.5}$–10^{38} erg s^{-1}, the UV/X-ray output from shock-ejecta interaction can be enough to power the observed dust luminosity (~1.0×10^{38} erg s^{-1}) measured by JWST on day 11 280. Furthermore, as found by Dessart & Hillier (2022) and Dessart et al. (2023), even modest stellar winds can build up and result in a relatively large UV flux at late times, generating a constant shock power of about 10^{40} erg s^{-1} in a standard Type II SN. Depending on the optical depth of the ejecta, back-scattered UV photons may be able to effectively heat not only circumstellar (pre-existing) dust but also newly formed grains located in the inner ejecta, as was discussed in more detail in Shahbandeh et al. (2023). Nevertheless,

we note that collecting direct observational UV evidence for the latter option seems to be quite challenging at such late epochs.

Finally, taking a closer look at the Galactic SNR Cas A could be helpful for understanding the dust origin and heating mechanisms in the case of SN 1993J (and in other Type IIb explosions). Studying the dust content of Cas A has been the topic of numerous studies (e.g., Dwek & Arendt 2008; Dunne et al. 2009; Barlow et al. 2010; Arendt et al. 2014; Bevan et al. 2017; De Looze et al. 2017; Priestley et al. 2019, 2022; Kirchschlager et al. 2023, 2024), and the object has also been a target of recent JWST observations (Milisavljevic et al. 2024). While many exciting details in the structure and ongoing interaction processes of this nearby SNR have been observed, there are efforts to understand its past and the fate of SNe IIb in general. SN 1993J, already in the transitional phase between an SN and an SNR, is an ideal object for follow-up studies from this perspective as well.

The cited studies present detailed investigations of the physical composition of the dust in both the ejecta and the ambient swept-up medium of Cas A. A general conclusion of these investigations is that the mid-IR component of Cas A's spectrum basically emerges from the post-shocked ejecta region, which contains a few $\times 10^{-3}$ $M_\odot$ of dust. This value is in good agreement with the one we found during the analysis of our current JWST data of SN 1993J. It may indicate that the dust we see now in SN 1993J can also be in the post-shocked ejecta. Furthermore, as these studies suggest, a much larger amount ($\sim$0.1–1.0 $M_\odot$) of very cold (<100 K) dust is located within the unshocked ejecta of Cas A. Following the arguments we described above, it could be possible that we see part of the heated unshocked ejecta dust in the mid-IR data of SN 1993J now, and this dust can cool well below 100 K after several decades (as the intensity of the CSM interaction decreases, which is suggested by the current trend seen in Fig. 5).

In the case of ejecta dust, the effect of grain-destruction processes caused by the reverse shock should be taken into account as well. This topic has been actively studied in the case of Cas A (e.g., Micelotta et al. 2016; De Looze et al. 2017; Priestley et al. 2022; Kirchschlager et al. 2023, 2024), especially because theoretical studies predict a small average grain size ($a < 0.01$ μm) in SN IIb ejecta (Nozawa et al. 2010; Biscaro & Cherchneff 2014, 2016). While all of these studies predict a very low survival rate of grains, the estimated rate values depend on various parameters (e.g., grain-size distribution, density contrast between the dust clumps and the ambient medium, and magnetic field strength) and seem to increase after some time (see the most recent calculations by Kirchschlager et al. 2023, 2024). However, as can be inferred from these studies, we note that the reverse shock may have hit only the outermost part of the ejecta of SN 1993J by now. Thus, the dust content in the inner part should not be affected yet. This is in agreement with our finding of similar dust masses in SN 1993J at ~15 and ~30 yr after explosion.

We also remark that the dust composition used to describe Cas A's IR-submillimeter spectra is mainly based on Al_2O_3 and various types of magnesium silicates (e.g., Arendt et al. 2014), but dust-synthesis models also allow for the presence of larger amounts of carbonaceous grains in SN IIb explosions (Nozawa et al. 2010; Biscaro & Cherchneff 2014, 2016). We note, however, that a lack of the characteristic silicate features does not necessarily mean that we do really see carbonaceous dust. It could also be very large silicate grains or high optical depths that quash the signs of silicate emission. A future JWST spectrum would be the necessary next step in revealing the true composition of dust in SN 1993J.

5. Conclusions

To summarize, analysis of recent JSWT/MIRI photometric data of SN 1993J suggests that it still contains a significant amount of dust ~30 yr after explosion. Comparing the current results to those of the analysis of earlier *Spitzer* data, we observed a similar amount ($\sim$0.01 $M_\odot$) of carbonaceous dust to that detected ~15–20 yr ago, but at a lower temperature (~120 K vs. ~165 K).

There are still open questions regarding whether we see the same dust and whether this dust has formed post-explosion (and is located in the inner or the post-shocked ejecta) or is pre-existing. As shown by Z22, this amount of dust can be entirely in the inner (unshocked) ejecta of SN 1993J, which is also supported by the red–blue line profile asymmetries of late-time optical spectra. In this case, it is possible that we see the same dust now (since we expect no grain destruction occurred in the unshocked region). This dust, if located in the inner ejecta, has presumably cooled over the years. This is also in agreement with the continuously decreasing intensity of the CSM interaction, which is assumed to be the main heating mechanism, even for ejecta dust (the presence of ongoing CSM interaction is revealed not just in the form of the long-lived Hα emission-line profile but also by a hot component in the recent JWST/MIRI SED of SN 1993J).

As another possibility (also shown by Z22), part or all of the observed dust (either pre-existing or newly formed) can be in the post-shocked regions of the SN. We observed such dust in the mid-IR in the ~350 yr-old remnant of Cas A in an amount similar to what was found in SN 1993J at a much younger age. In general, we have barely any information on the dust evolution in the SN-SNR transitional phase; however, one can assume (for example) continuous destruction and condensation of grains. Furthermore, we note that the dust amount ($\sim$0.01 $M_\odot$) found in SN 1993J based on JWST/MIRI data is comparable to dust masses seen in strongly interacting Type IIn SNe (e.g., Fox et al. 2011, 2013, 2020). Since we assume much lower mass-loss rates in SN IIb progenitors than in SN IIn ones, it may be an argument against entirely pre-existing dust in SN 1993J. However, most of the known SN IIn IR dust masses were determined from short-wavelength *Spitzer* data, and upcoming JWST observations of SNe IIn and uniform dust-modeling methods (especially on grain properties) are expected to achieve further progress in this field.

Moreover, beyond the local dust assumed in the close environment of SN 1993J, we may have identified signs of a potential IR echo (found as residual background emission in JWST/MIRI images after PSF subtraction) – that is, radiation of a more-distant dust shell heated by the SN shock-breakout luminosity. Nevertheless, to get a full picture of the dusty SN 1993J, it would be useful to obtain a complete near-IR and mid-IR spectrum at the same SN phase. Such a dataset would allow us to take into account further important aspects such as the effects of atomic and molecular line emission on the IR spectrum (see Milisavljevic et al. 2024, for the case of Cas A) or how the progenitor's binary companion affects the CSM geometry and the dust formation/heating processes (e.g., Fox et al. 2014; Kochanek 2017). All of these arguments, along with the results presented above, should make SN 1993J a promising spectroscopic target in future JWST cycles and the subject of further detailed studies.

Data availability

Data are available at the Barbara A. Mikulski Archive for Space Telescopes (MAST[3]).

[3] http://dx.doi.org/10.17909/tvxf-qh40

Acknowledgements. We thank our anonymous referee for valuable comments. This work is based on observations made with the NASA/ESA/CSA *James Webb Space Telescope*. The data were obtained from the Mikulski Archive for Space Telescopes at the Space Telescope Science Institute, which is operated by the Association of Universities for Research in Astronomy, Inc., under NASA contract NAS 5-03127 for JWST. These observations are associated with program SURVEY 3921. This project has been supported by the NKFIH OTKA FK-134432 grant of the National Research, Development and Innovation (NRDI) Office of Hungary. S.Z. is supported by the ÚNKP-23-4-SZTE-574 New National Excellence Program of the Ministry for Culture and Innovation from the source of the NRDI Fund, Hungary. I.D.L. has received funding from the European Research Council (ERC) under the European Union's Horizon 2020 research and innovation programme DustOrigin (ERC-2019-StG-851622) and the Belgian Science Policy Office (BELSPO) through the PRODEX project "JWST/MIRI Science exploitation" (C4000142239). A.V.F. is grateful for financial support from the Christopher R. Redlich Fund and many other donors. C.A. acknowledges support by NASA JWST grants GO-02114, GO-02122, GO-03726, GO-04436, and GO-04522. Some of the data presented herein were obtained at the W. M. Keck Observatory, which is operated as a scientific partnership among the California Institute of Technology, the University of California, and NASA; the observatory was made possible by the generous financial support of the W. M. Keck Foundation.

References

Aldering, G., Humphreys, R. M., & Richmond, M. 1994, AJ, 107, 662
Arendt, R. G., Dwek, E., Kober, G., Rho, J., & Hwang, U. 2014, ApJ, 786, 55
Arendt, R. G., Dwek, E., Bouchet, P., et al. 2016, AJ, 151, 62
Arendt, R. G., Dwek, E., Bouchet, P., et al. 2020, ApJ, 890, 2
Baer-Way, R., DeGraw, A., Zheng, W., et al. 2024, ApJ, 964, 172
Barlow, M. J., Krause, O., Swinyard, B. M., et al. 2010, A&A, 518, L138
Bartel, N., Bietenholz, M. F., Rupen, M. P., et al. 2002, ApJ, 581, 404
Bevan, A., Barlow, M. J., & Milisavljevic, D. 2017, MNRAS, 465, 4044
Bietenholz, M. F., Bartel, N., & Rupen, M. P. 2001, ApJ, 557, 770
Bietenholz, M. F., Bartel, N., & Rupen, M. P. 2003, ApJ, 597, 374
Biscaro, C., & Cherchneff, I. 2014, A&A, 564, A25
Biscaro, C., & Cherchneff, I. 2016, A&A, 589, A132
Bouchet, P., Dwek, E., Danziger, J., et al. 2006, ApJ, 650, 212
Bouchet, P., García-Marín, M., Lagage, P. O., et al. 2015, PASP, 127, 612
Chandra, P., Dwarkadas, V. V., Ray, A., Immler, S., & Pooley, D. 2009, ApJ, 699, 388
Cohen, J. G., Darling, J., & Porter, A. 1995, AJ, 110, 308
De Looze, I., Barlow, M. J., Swinyard, B. M., et al. 2017, MNRAS, 465, 3309
De Looze, I., Barlow, M. J., Bandiera, R., et al. 2019, MNRAS, 488, 164
Dessart, L., & Hillier, D. J. 2022, A&A, 660, L9
Dessart, L., Gutiérrez, C. P., Kuncarayakti, H., Fox, O. D., & Filippenko, A. V. 2023, A&A, 675, A33
Draine, B. T., & Li, A. 2007, ApJ, 657, 810
Dunne, L., Maddox, S. J., Ivison, R. J., et al. 2009, MNRAS, 394, 1307
Dwek, E., & Arendt, R. G. 2008, ApJ, 685, 976
Dwek, E., Galliano, F., & Jones, A. P. 2007, ApJ, 662, 927
Dwek, E., Arendt, R. G., Bouchet, P., et al. 2010, ApJ, 722, 425
Dwek, E., Sarangi, A., & Arendt, R. G. 2019, ApJ, 871, L33
Fabbri, J., Otsuka, M., Barlow, M. J., et al. 2011, MNRAS, 418, 1285
Filippenko, A. V. 1982, PASP, 94, 715
Filippenko, A. V. 1988, AJ, 96, 1941
Filippenko, A. V. 1997, ARA&A, 35, 309
Filippenko, A. V., Matheson, T., & Ho, L. C. 1993, ApJ, 415, L103
Fox, O. D., Chevalier, R. A., Dwek, E., et al. 2010, ApJ, 725, 1768
Fox, O. D., Chevalier, R. A., Skrutskie, M. F., et al. 2011, ApJ, 741, 7
Fox, O. D., Filippenko, A. V., Skrutskie, M. F., et al. 2013, AJ, 146, 2
Fox, O. D., Azalee Bostroem, K., Van Dyk, S. D., et al. 2014, ApJ, 790, 17
Fox, O. D., Fransson, C., Smith, N., et al. 2020, MNRAS, 498, 517
Fransson, C., & Kozma, C. 2002, New A Rev., 46, 487
Freedman, W. L., Madore, B. F., Gibson, B. K., et al. 2001, ApJ, 553, 47
Gomez, H. L., Krause, O., Barlow, M. J., et al. 2012, ApJ, 760, 96
Hildebrand, R. H. 1983, QJRAS, 24, 267
Indebetouw, R., Matsuura, M., Dwek, E., et al. 2014, ApJ, 782, L2
Jones, O. C., Kavanagh, P. J., Barlow, M. J., et al. 2023, ApJ, 958, 95
Kirchschlager, F., Schmidt, F. D., Barlow, M. J., De Looze, I., & Sartorio, N. S. 2023, MNRAS, 520, 5042
Kirchschlager, F., Sartorio, N. S., De Looze, I., et al. 2024, MNRAS, 528, 5364
Kochanek, C. S. 2017, MNRAS, 471, 3283
Kotak, R., Meikle, W. P. S., Farrah, D., et al. 2009, ApJ, 704, 306
Krause, O., Rieke, G. H., Birkmann, S. M., et al. 2005, Science, 308, 1604
Krause, O., Birkmann, S. M., Usuda, T., et al. 2008, Science, 320, 1195
Kundu, E., Lundqvist, P., Sorokina, E., et al. 2019, ApJ, 875, 17
Larsson, J., Fransson, C., Sargent, B., et al. 2023, ApJ, 949, L27
Lewis, J. R., Walton, N. A., Meikle, W. P. S., et al. 1994, MNRAS, 266, L27
Liu, J.-F., Bregman, J. N., & Seitzer, P. 2003, ApJ, 582, 919
Martí-Vidal, I., Marcaide, J. M., Alberdi, A., et al. 2011, A&A, 526, A142
Matheson, T., Filippenko, A. V., Ho, L. C., Barth, A. J., & Leonard, D. C. 2000, AJ, 120, 1499
Matsuura, M., Dwek, E., Meixner, M., et al. 2011, Science, 333, 1258
Matsuura, M., De Buizer, J. M., Arendt, R. G., et al. 2019, MNRAS, 482, 1715
Matthews, K., Neugebauer, G., Armus, L., & Soifer, B. T. 2002, AJ, 123, 753
Maund, J. R., & Smartt, S. J. 2009, Science, 324, 486
Maund, J. R., Smartt, S. J., Kudritzki, R. P., Podsiadlowski, P., & Gilmore, G. F. 2004, Nature, 427, 129
Meikle, W. P. S., Kotak, R., Farrah, D., et al. 2011, ApJ, 732, 109
Micelotta, E. R., Dwek, E., & Slavin, J. D. 2016, A&A, 590, A65
Milisavljevic, D., & Fesen, R. A. 2017, in Handbook of Supernovae, eds. A. W. Alsabti, & P. Murdin, 2211
Milisavljevic, D., Fesen, R. A., Chevalier, R. A., et al. 2012, ApJ, 751, 25
Milisavljevic, D., Temim, T., De Looze, I., et al. 2024, ApJ, 965, L27
Nomoto, K., Suzuki, T., Shigeyama, T., et al. 1993, Nature, 364, 507
Nozawa, T., Kozasa, T., Tominaga, N., et al. 2010, ApJ, 713, 356
Oke, J. B., Cohen, J. G., Carr, M., et al. 1995, PASP, 107, 375
Perley, D. A. 2019, PASP, 131, 084503
Perrin, M. D., Sivaramakrishnan, A., Lajoie, C. P., et al. 2014, in Space Telescopes and Instrumentation 2014: Optical, Infrared, and Millimeter Wave, eds. J. Oschmann, M. Jacobus, M. Clampin, G. G. Fazio, & H. A. MacEwen, SPIE Conf. Ser., 9143, 91433X
Pierel, J. 2024, https://doi.org/10.5281/zenodo.12100100
Priestley, F. D., Barlow, M. J., & De Looze, I. 2019, MNRAS, 485, 440
Priestley, F. D., Arias, M., Barlow, M. J., & De Looze, I. 2022, MNRAS, 509, 3163
Ressler, M. E., Sukhatme, K. G., Franklin, B. R., et al. 2015, PASP, 127, 675
Rest, A., Pierel, J., Correnti, M., et al. 2023, https://doi.org/10.5281/zenodo.7892935
Richardson, D., Branch, D., & Baron, E. 2006, AJ, 131, 2233
Rieke, G., & Wright, G. 2022, Nat. Astron., 6, 891
Rieke, G. H., Wright, G. S., Böker, T., et al. 2015, PASP, 127, 584
Sarangi, A. 2022, A&A, 668, A57
Sarangi, A., & Cherchneff, I. 2015, A&A, 575, A95
Seitenzahl, I. R., Timmes, F. X., & Magkotsios, G. 2014, ApJ, 792, 10
Shahbandeh, M., Sarangi, A., Temim, T., et al. 2023, MNRAS, 523, 6048
Sibthorpe, B., Ade, P. A. R., Bock, J. J., et al. 2010, ApJ, 719, 1553
Smith, N., Li, W., Filippenko, A. V., & Chornock, R. 2011, MNRAS, 412, 1522
Smith, N., Kilpatrick, C. D., Mauerhan, J. C., et al. 2017, MNRAS, 466, 3021
Sugerman, B. E. K., & Crotts, A. P. S. 2002, ApJ, 581, L97
Sugerman, B. E. K., Andrews, J. E., Barlow, M. J., et al. 2012, ApJ, 749, 170
Szalai, T., & Vinkó, J. 2013, A&A, 549, A79
Szalai, T., Vinkó, J., Balog, Z., et al. 2011, A&A, 527, A61
Szalai, T., Zsíros, S., Fox, O. D., Pejcha, O., & Müller, T. 2019, ApJS, 241, 38
Szalai, T., Fox, O. D., Arendt, R. G., et al. 2021, ApJ, 919, 17
Tanaka, M., Nozawa, T., Sakon, I., et al. 2012, ApJ, 749, 173
Temim, T., & Dwek, E. 2013, ApJ, 774, 8
Tinyanont, S., Kasliwal, M. M., Fox, O. D., et al. 2016, ApJ, 833, 231
Van Dyk, S. D. 2013, AJ, 145, 118
Van Dyk, S. D., Garnavich, P. M., Filippenko, A. V., et al. 2002, PASP, 114, 1322
Weiler, K. W., Williams, C. L., Panagia, N., et al. 2007, ApJ, 671, 1959
Wesson, R., Barlow, M. J., Matsuura, M., & Ercolano, B. 2015, MNRAS, 446, 2089
Zsíros, S., Nagy, A. P., & Szalai, T. 2022, MNRAS, 509, 3235
Zsíros, S., Szalai, T., De Looze, I., et al. 2024, MNRAS, 529, 155
Zubko, V., Dwek, E., & Arendt, R. G. 2004, ApJS, 152, 211

[1] Department of Experimental Physics, Institute of Physics, University of Szeged, Dóm tér 9, 6720 Szeged, Hungary
[2] MTA-ELTE Lendület "Momentum" Milky Way Research Group, Szent Imre H. st. 112, 9700 Szombathely, Hungary
[3] Department of Physics and Astronomy, Johns Hopkins University, Baltimore, MD 21218, USA
[4] Space Telescope Science Institute, 3700 San Martin Drive, Baltimore, MD 21218, USA
[5] DARK, Niels Bohr Institute, University of Copenhagen, Jagtvej 128, 2200 Copenhagen, Denmark
[6] Department of Astrophysical Sciences, Princeton University, Princeton, NJ 08544, USA

[7] Sterrenkundig Observatorium, Ghent University, Krijgslaan 281 – S9, 9000 Gent, Belgium
[8] Steward Observatory, University of Arizona, 933 N. Cherry St, Tucson, AZ 85721, USA
[9] Department of Astronomy, University of California, Berkeley, CA 94720-3411, USA
[10] Caltech/IPAC, Mailcode 100-22, Pasadena, CA 91125, USA
[11] Gemini Observatory, 670 N. Aohoku Place, Hilo, Hawaii 96720, USA
[12] Department of Physics, Virginia Tech, Blacksburg, VA 24061, USA
[13] Department of Physics & Astronomy, Louisiana State University, Baton Rouge, LA 70803, USA
[14] Institut d'Astrophysique de Paris, CNRS–Sorbonne Université, 98 bis boulevard Arago, F-75014 Paris, France
[15] NASA at Goddard Space Flight Center, Code 665, Greenbelt, MD 20771, USA
[16] Center for Astrophysics | Harvard & Smithsonian, 60 Garden Street, Cambridge, MA 02138-1516, USA
[17] Oskar Klein Centre, Department of Physics, Stockholm University, AlbaNova SE-10691 Stockholm, Sweden
[18] Purdue University, Department of Physics and Astronomy, 525 Northwestern Ave, West Lafayette, IN 47907, USA
[19] Integrative Data Science Initiative, Purdue University, West Lafayette, IN 47907, USA
[20] Department of Astronomy and Astrophysics, University of California, Santa Cruz, CA 95064, USA
[21] National Astronomical Research Institute of Thailand, 260 Moo 4, Donkaew, Maerim Chiang Mai 50180, Thailand
[22] MIT-Kavli Institute for Astrophysics and Space Research, 77 Massachusetts Ave., Cambridge, MA 02139, USA
[23] Cahill Center for Astrophysics, California Institute of Technology, 1200 E. California Blvd., Pasadena, CA 91125, USA
[24] NSF's NOIRLab, 950 N. Cherry Avenue, Tucson 85719, AZ, USA
[25] European Space Agency (ESA), ESAC, 28692 Villanueva de la Canada, Madrid, Spain
[26] Department of Astronomy, University of Virginia, Charlottesville, VA 22904-4325, USA
[27] X-ray Astrophysics Laboratory, NASA/Goddard Space Flight Center (GSFC), Greenbelt, MD 20771, USA
[28] Department of Physics, College of Physical Sciences and Technology, Hebei University, Wusidong Road 180, Baoding 071002, China
[29] Department of Physics, College of Physical Sciences and Technology, Hebei University, Wusidong Road 180, Baoding 071002, China

Appendix A: Modeling the JWST/MIRI SED of SN 1993J assuming large dust grains

In Fig. A.1 we present the best-fit two-component models assuming a hot BB and a cold dust component consists of large grains (a=1.0 and 5.0 μm amC, and a=5.0 μm silicate dust, respectively), together with the adopted κ_λ curves. We applied this set of fittings only to the average values of the observed JWST/MIRI fluxes. Models using a=1.0 amC dust result in very similar parameters to that of the basic set we used (a=0.1 amC dust, see Table 2), while both a=5.0 μm amC and silicate dust models also result in similar cold dust and hot BB temperatures ($T_{\rm cold} \sim 110-140$ K, and $T_{\rm BB,warm} \sim 370-420$ K, respectively), but in smaller cold dust masses ($\sim 10^{-3}$ M$_\odot$). Nevertheless, as we described above, such large grains are not expected in SN 1993J at this phase and, furthermore, this dataset does not allow us to truly disentangle models with different grain-size distributions.

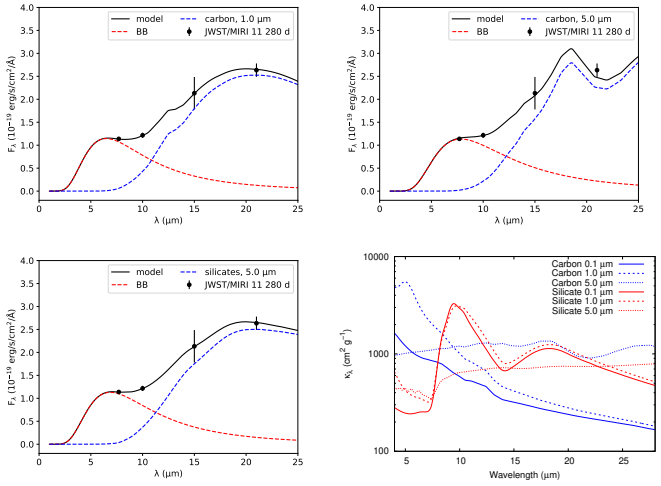

Fig. A.1. Best-fit two-component models assuming a hot BB and a cold dust component: amC, a=1.0 μm (*top left*), amC, a=5.0 μm (*top right*), silicate, a=5.0 μm (*bottom left*), and the adopted κ_λ values (*bottom right*).

Appendix B: PSF residuals in JWST/MIRI images

The two figures we present here refer to the potential local background emission we identified at the SN site as residuals after PSF subtraction (see Sec. 3.3). We first examine the quality of the PSF subtraction for multiple isolated stars to ensure the residual emission is not a result of inaccuracies in the PSF models obtained with `WebbPSF`.

Figure B.1 compares the results of PSF removal from a bright star and a faint star, located at respective positions of (α, δ) = ($09^{\rm hr}55^{\rm m}24.86^{\rm s}$, +69°01′07.2″) and ($09^{\rm hr}55^{\rm m}23.27^{\rm s}$, +69°01′01.7″), along with SN 1993J in the F1500W images. While the bright star shows noticeable PSF residuals, these are $\lesssim$ 3% of the peak of the star and do not show the prominent "ring" pattern that is evident in the SN 1993J residuals at up to $\sim$ 20% of the source flux. The faint-star PSF subtracts cleanly, with any PSF residuals below the noise level. This comparison clearly indicates that the residuals around SN 1993J are not due to inaccuracies in the PSF model, but instead arise from real emission in the local SN environment. We note that the "ring"/doughnut morphology seen here is an artefact of using a large fitting box that results in oversubtraction of the background

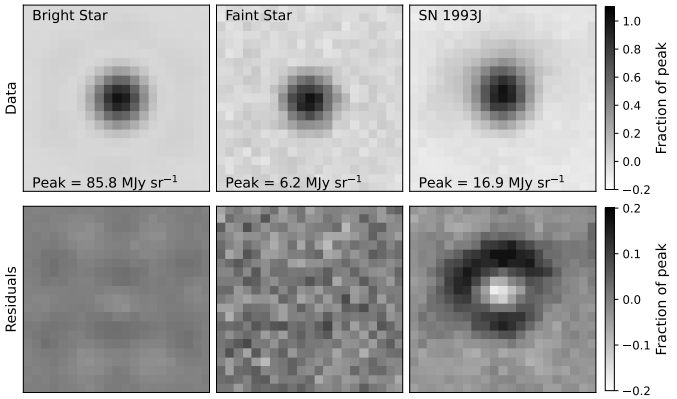

Fig. B.1. Comparison of subtracting the `WebbPSF` models from a bright star (left), a faint star (center), and SN 1993J (right) in F1500W images.

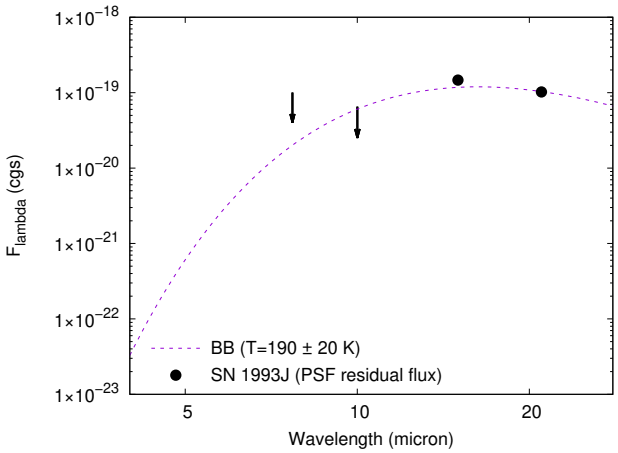

Fig. B.2. Best-fitting BB curve (dashed purple) to integrated PSF residual fluxes (black circles) and upper limits (black arrows).

in the core of the PSF (see Sec. 3.3 for more careful background estimation and PSF fitting).

In Fig. B.2, we show the integrated residual fluxes (F1500W=0.11±0.01 mJy and F2100W = 0.14±0.01 mJy, see Sec. 3.3) and upper limits (20 μJy for both F770W and F1000W filter images) for the background emission around SN 1993J, together with a fit BB curve to estimate the temperature of the emitting source. Residual fluxes and upper limits were determined by a simple summation of fluxes within 14 × 14 pixel boxes that cover the residual structures of the PSF in the F1500W and F2100W images, but exclude light from nearby point sources. The BB fit suggests a dust temperature of $\sim$ 190 ± 20 K.